Molecular Simulation
Vol. 00, No. 0, 2012, 1–5

Taylor & Francis
Taylor & Francis Group

Internal carburisation of an industrial alloy: a quantum chemical study of microstructure's changes

C. Lanz[a], G. Brizuela[b] and S. Simonetti[b,c]*

[a]*Departamento de Ingeniería, Universidad Nacional del Sur, Av. Alem 1253, 8000 Bahía Blanca, Argentina;* [b]*Departamento de Física, IFISUR, Universidad Nacional del Sur-CONICET, Av. Alem 1253, 8000 Bahía Blanca, Argentina;* [c]*Departamentos de Ciencias Básicas e Ingeniería Mecánica, Facultad Regional Bahía Blanca, Universidad Tecnológica Nacional, 11 de Abril 461, 8000 Bahía Blanca, Argentina*

(*Received 7 May 2012; final version received 6 June 2012*)

A quantum chemical theoretical study on the chemical bonding and electronic structure of the γ-FeNiCr–C interaction is performed using the Atom Superposition and Electron Delocalisation method in order to contribute to the understanding of the changes in the alloy microstructure caused by carburisation phenomenon. A complementary analysis of a HK-40 structure changes after service is also presented by using optical and electron microscopy techniques.

Keywords: computational techniques; iron–nickel–chromium alloy; carburisation; microanalysis techniques

Introduction

High-temperature corrosion is generally known as a material degradation process that occurs at the surface of engineering components. In the case of internal corrosion, the corrosive species penetrates into the material by solid-state diffusion leading to the formation of internal precipitates, for instance, oxides (internal oxidation), nitrides (internal nitridation) and carbides (carburisation). It is known from numerous publications and technical failure cases that internal corrosion results in a strong deterioration of the properties of a material. The mechanisms and kinetics of internal corrosion processes are determined by the temperature, the local chemical composition of the material, the solubility and diffusivity of the corrosive species as well as the mechanical loading conditions [1].

The initiation of stress corrosion cracking in face-centred cubic (FCC) Fe–Cr–Ni ternary alloys has been studied by means of quantum chemical molecular dynamics at 288°C. This study showed that the iron and chromium atoms segregate faster than nickel atoms at the surfaces [2]. Diffusion thermodynamic and kinetic information for dilute Ni–Cr and Ni–Fe alloys via *ab initio* techniques has showed that the faster Cr diffusivity is likely related to Cr depletion at grain boundaries under irradiation [3,4].

Ferritic steels at temperatures above 950°C suffer precipitation of carbides (M_3C, M_6C and $M_{23}C_6$, where M is a mixture of metallic atoms) during the subsequent cooling, and this causes a decrease in both toughness and corrosion resistance [5].

Fe-base alloys in CH_4/H_2 carburising gas at 800°C suffer external carburisation and oxidation, and the external Cr-rich scale layers were continuous consisting of oxides and carbides. Carburisation resistance primarily depends on the protection afforded by external continuous layers. At 1100°C, extensive external carburisation occurred, and external layers became discontinuous consisting of Cr/Fe-carbides or metallic CrFe phases [6].

Thermodynamic equilibrium calculations have been conducted to understand the carburising environment of ethylene pyrolysis in petrochemical industries. Calculated equilibrium has been estimated to be in the range of 10–101 atm for the operating condition. In this environment, chromium oxide was stable for up to 1030–1040°C. However, Cr was converted to chromium carbides such as Cr_7C_3 and Cr_2C_3 above 1030–1040°C. More than 25mass%Cr was necessary for austenitic alloys to provide protection against carburisation environments at 1000°C. At 1100 and 1150°C, Cr scale did not provide protection. Alloy of Fe-25%Cr-38%Ni-l.8%Si-l.5%Mo had excellent carburisation resistance similar to Fe-32%Cr-43%Ni-1.7%Si cast alloy in the laboratory tests [7].

Crack propagation and oxidation phenomena during high-temperature service (up to 25,000 h) of tubes made from HK-40 alloy have been investigated. The service conditions subjected the materials to oxidising and carburising conditions on the surfaces leading to the formation of complex oxide structures in both external and internal oxide scales, and of carbide-denuded zones in subsurface regions [8].

The events leading to the failure of HP ethylene pyrolysis heater tubing have been examined by Chauhan et al. X-ray maps indicate that a complex oxide coating, which inhibits carbon diffusion, forms on the process side

*Corresponding author. Email: ssimonet@uns.edu.ar

ISSN 0892-7022 print/ISSN 1029-0435 online
© 2012 Taylor & Francis
http://dx.doi.org/10.1080/08927022.2012.701745
http://www.tandfonline.com

of the tubing during service. Phase equilibrium studies predict that even without C diffusion process, metal carbides will precipitate out of the FCC matrix. It was estimated that a 6-mm thick tube operating at 1100°C would completely carburise in 2 years if the protective coating is damaged [9].

Ethylene pyrolysis in the petrochemical industries is considered as the most important process for producing chemical products. Reformer tubes are generally made from cast creep-resistant austenitic steel HK grade. Although the furnace tubes are usually designed for a normal life of 100,000 h (11.4 years), their actual service life, however, varies from 30,000 to 180,000 h, depending on the service conditions. Due to prolonged exposure to high temperature, the microstructure of the material is subjected to degradation. In this paper, we have studied the HK-40 alloy carburisation by modelling a γ-FeNiCr–C cluster and performing calculations using the Atom Superposition and Electron Delocalisation Molecular Orbital (ASED-MO) method. The changes in the alloy's electronic structure after the carbon location process are addressed. The chemical bonding analysis is also considered in order to explain some failures observed experimentally in the HK-40 alloy. In addition, we provided a related analysis of the changes in the HK-40 microstructure (30,000 h of service at 800–1150°C) due to carburisation process, using optical and scanning electron microscopy.

Result and discussion

A computational study has been performed to analyse the changes in the electronic structure and the chemical bonding for the carbon–alloy interaction during carburisation phenomena. In order to simulate the HK-40 alloy, we modelled a cluster with γ-FeNiCr structure containing 99 atoms of iron, 45 atoms of Cr and 36 atoms of Ni, distributed in five layers stacking (110) planes. The calculations have been performed using the ASED-MO method [10–13]. The modification of the extended Hückel molecular orbital method was implemented with the YAeHMOP program [14]. To understand the interactions between the atoms, we used the concept of crystal orbital overlap population (COOP) curves. The COOP curve is a plot of the overlap population weighted density of states (DOS) versus energy. The integration of the COOP curve up to the Fermi level (E_f) gives the total overlap population of the bond specified, and it is a measure of the bond strength.

We performed calculations to compare the FeNiCr-based alloy structure before and after the C location. According to that, we localised the C atom in the FeNiCr matrix finding their minimum energy position. Figure 1(a) shows the DOS corresponding to the isolated FeNiCr system. The alloy d states form a band starting at − 14 eV and with a bandwidth of 8 eV, while the s and p states are scattered and penetrating the d band. Figure 1(b) shows the

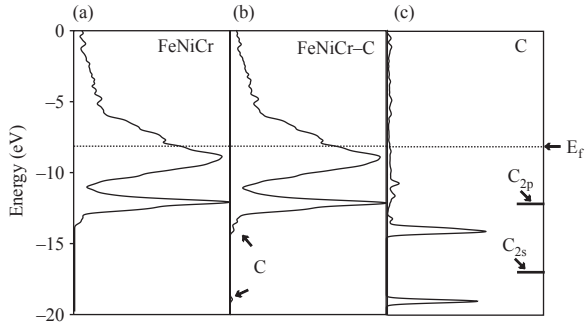

Figure 1. (a) Total DOS for isolated FeNiCr cluster, (b) total DOS for FeNiCr–C cluster and (c) projected DOS for the C atom in the FeNiCr–C cluster (the horizontal lines correspond to C states before adsorption).

FeNiCr system after the C location, we can see the position of the C states after adsorption. The small contribution of C to DOS is due to its low concentration. A major view of C impurity states can be seen in Figure 1(c). The C projected DOS plot shows some deep C s–p states centred at lower energy values showing that the C adsorption process is favoured. The value of the Fermi energy (E_f) is − 8.22 eV. We found no significant change in the E_f because the total DOS is dominated by the FeNiCr matrix so that the changes are small.

The C atom locates near Ni, Fe and Cr atoms at distances of 1.38, 1.41 and 1.73 Å, respectively. As a consequence, Ni–C, Fe–C and Cr–C interactions are formed. The COOP curves for the C-metal interactions and a schematic view of the C adsorption zone are shown in Figure 2. As we can see, the C metals are mainly bonding

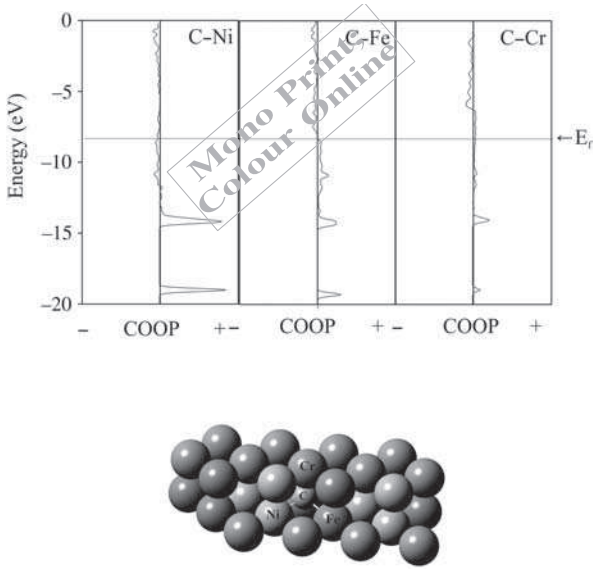

Figure 2. COOP curves for C–Ni, C–Fe and C–Cr interactions in the FeNiCr–C cluster. A view of the C location zone is schematised.

[Q23] Table 1. Atomic orbital occupations for the C atom and their neighbouring atoms.

Atom	s	p_x	p_y	p_z	$d_{x^2-y^2}$	d_{z^2}	d_{xy}	d_{xz}	d_{yz}
Ni	0.7783	0.3375	0.3562	0.3924	1.8784	1.7612	1.8789	1.8187	1.8065[a]
	0.9482	0.3793	0.3785	0.3751	1.8824	1.8659	1.8803	1.9064	1.9007[b]
Fe	0.5322	0.0295	0.0510	0.0353	1.1682	1.0740	1.0791	1.2523	1.1983[a]
	0.6459	0.0601	0.0698	0.0623	1.3508	1.3382	1.3421	1.2143	1.2656[b]
Cr	0.4739	0.0531	0.0240	0.0424	0.5106	0.6140	0.6483	0.5649	0.5541[a]
	0.5497	0.0622	0.0406	0.0564	0.5473	0.6838	0.6781	0.5652	0.5567[b]
C	1.3539	1.2067	1.1269	1.2272[a]	–	–	–	–	–

[a] In the FeNiCr–C cluster. [b] In the FeNiCr-isolated cluster.

Table 2. Chemical composition of the as-cast HK-40 alloy (wt.%).

	C	Si	Mn	Cr	Ni	Mo	Fe
HK-40	0.4	1.7	1.4	24.6	20.4	<0.5	Balance[a]

[a] Spectromax analysis for the specimens used.

interactions and the biggest C metal OP corresponds to the C–Ni interaction (C–Ni > C–Fe > C–Cr).

The atomic orbital occupations of the C nearest neighbour metallic atoms are modified after the C location. The electron densities of the atoms involved in the C-metal interactions are summarised in Table 1. The Ni 4s population decreases to about 18% when the C is present. The Ni 4p [Q4] populations decrease to 4%, while the Ni 3d populations diminish to about 2%. This indicates a majority participation of Ni 4s orbital in the C—Ni bonding. However, the Fe 4s population decreases to about 18% when the C is present (see Table 2). The Fe 4p populations decrease to about 40%, the p_x and p_z orbitals are the most affected. The Fe 3d population decreases to about 11%. This denoted a greater participation of Fe 4p orbital in the C—Fe bonding. In the [Q5] case of the Cr atom nearest neighbour to C, the Cr 4s population decreases to about 14%, and the contribution of Cr 4p populations decrease to 25%, presenting the Cr 4 p_y orbital the majority participation in the C—Cr bonding,

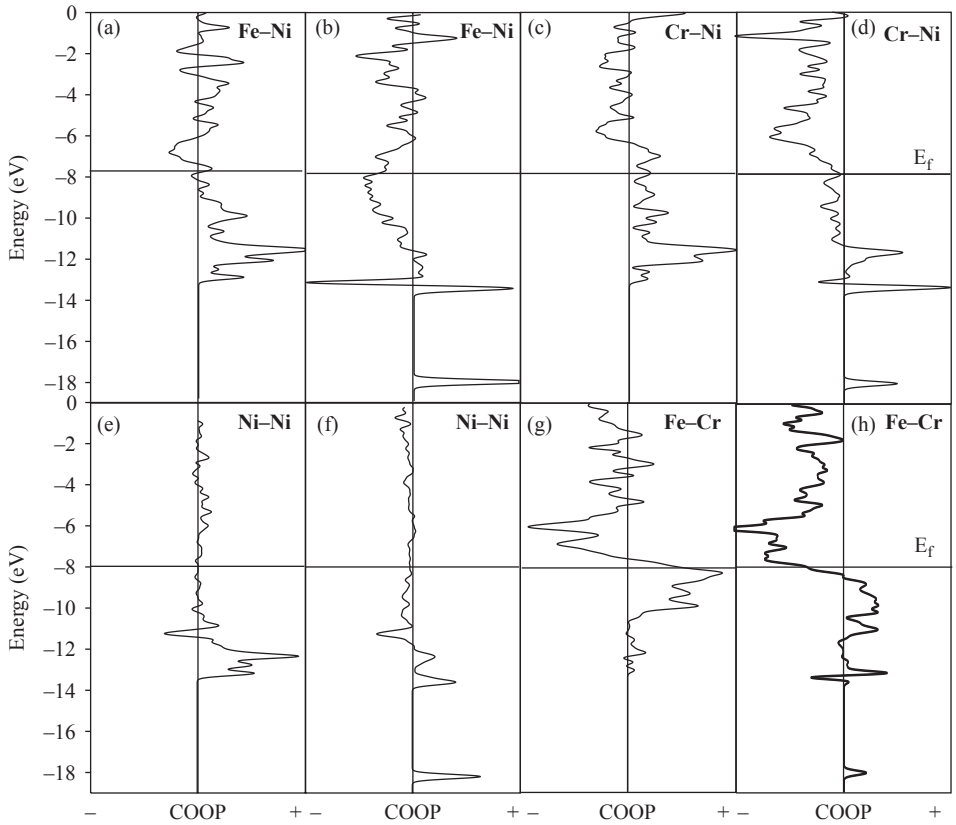

Figure 3. COOP curves for Fe—Ni bond, (a) before and (b) after C location. COOP curves for Cr—Ni bond, (c) before and (d) after C location. COOP curves for Ni—Ni bond, (e) before and (f) after C location. COOP curves for Fe—Cr bond, (g) before and (h) after C location.

while the Cr 3d populations diminish to about 5%. As predicted by the electronegativity differences, the Mulliken population analysis brings a partial negative charge on the C atom, whereas a positive charge on the close neighbour Ni, Fe and Cr atoms, indicating an electron transfer to the C atom from the Ni, Fe and Cr nearest neighbour atoms. We observed the most important electron transfer corresponding to Fe nearest neighbour atom.

The metallic bonds strength is modified after the C location. The Fe—Ni, Cr—Ni, Ni—Ni and Fe—Cr bonds nearest neighbours to C atom are the most affected; their OPs diminish to 85%, 75%, 69% and 64%, respectively. The nearest neighbour Fe—Fe and Cr—Cr bond strengths decrease to 9% and 1%, respectively. Figure 3 shows the metal–metal interactions, before and after the C location. We can associate the observed OP diminish with the metallic bond weakening that is mainly a consequence of the new C-metal interactions.

The changes in the structure can also be observed by optical and electron microscopy techniques. When we compared two samples of the HK-40, the as-cast (see alloy composition in Table 2) with the ex-service conditions obtained of the tubes of the cracking furnace from a petrochemical plant after 30,000 h of service at 800–1150°C, we observe that the two microstructure finenesses are very different after a so long service at these operating conditions. We can observe the as-cast alloy microstructure corresponding to an austenitic matrix where long carbides of type M_7C_3 (M = metal) are presented. Carbides are preferentially located, in dendritic edges in the form of 'necklace' surrounding to the austenitic phase and in the grain edges, showing a partial precipitation (Figure 4(a)). In the service-exposed alloy, great coalescence of carbides of bigger size decorating the austenitic matrix is observed (Figure 4(b)). From the service-exposed material SEM analysis, the appearance of intragranular carbides in the alloy is observed (Figure 4(c)). Carbide agglutination become visible in the grain edge, and it generates a state of internal tension due to their size. Cavities oriented between grains and some microfissures are originated in grain edges. This could indicate that the material presents damage by creep.

The intrinsic existence of porosities and cracks contribute to reduce the effort propagation towards the substrate, since they act as points of nucleation and crack propagation. The main effect of the thermal fatigue is characterised by the formation of cracks that propagate by effort changes due to thermal cycle effects, which can appear when the deformations are generated by the growth of the carbides and the difference in the thermal expansion coefficients. In this type of alloys, the carbon is generally present in proportions from 0.05% to 2%. The elements presenting in the matrix react with carbon and form different types of carbides that can be classified in frequent carbides of type MC, M_6C and $M_{23}C_6$ presenting from temperatures near 815°C and less regular carbides of type

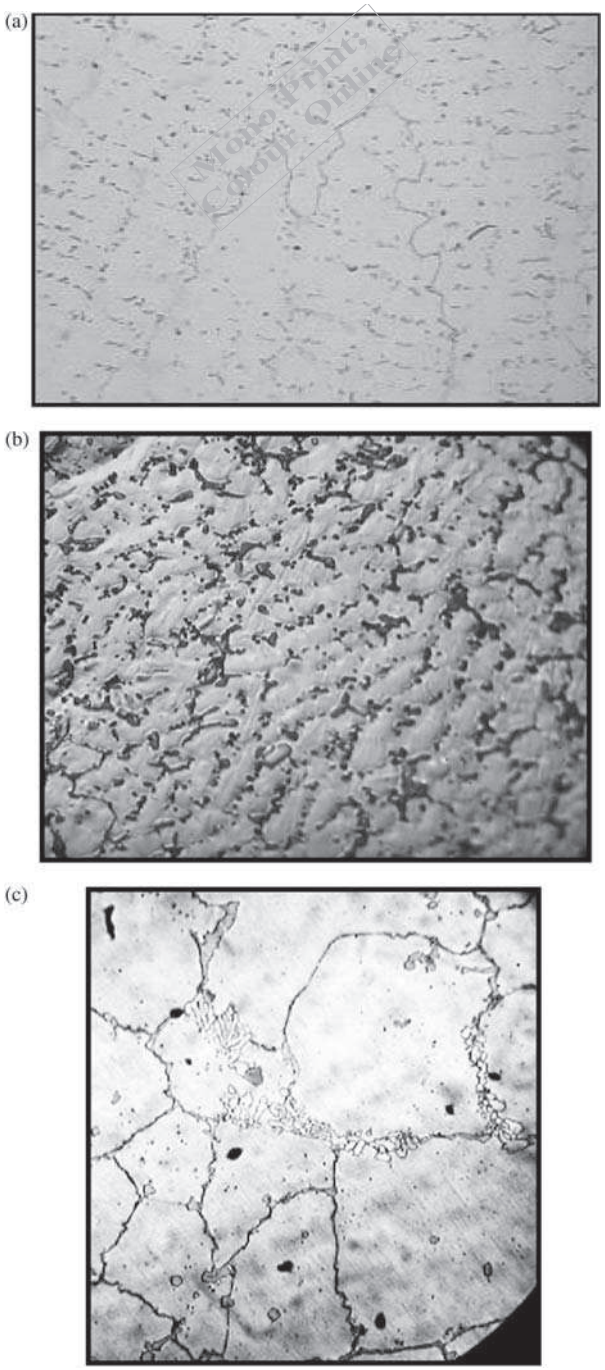

Figure 4. Optical micrographs of (a) the as-cast HK-40 alloy (160 ×) and (b) the HK-40 alloy tested at 800–1150°C during 30,000 h (200 ×). (c) SEM micrographs of the HK-40 alloy tested at 800–1150°C during 30,000 h (1000 ×).

M_7C_3, M_3C and $M_{13}C$ [15]. Carbides MC have FCC highly stable structure and are heterogeneously distributed through the alloy in the form of extended precipitates. This type of carbides tends to completely disappear after many hours of operation (>5000) degrading itself to form carbides of the type $M_{23}C_6$. This type of carbides normally precipitates throughout the grain boundaries like small

particles; the size increases progressively as the time passes. Carbides of type M_6C precipitate in the grain edges when the temperatures are between 815°C and 980°C. All this detected carbides can be justified at a microscopic level by simplified previous theoretical calculations regarding metal-C chemical interactions; in addition, the loss of mechanical properties is directly related to the decrease of metal–metal bonding in favour of forming metal-C species.

Conclusions

This investigation provided an atomistic modelling to better elucidate the mechanism of stress corrosion cracking of iron–nickel–chromium alloys exposed to high temperature. The theoretical calculations help us to interpret the changes in the alloy electronic structure and the chemical bonding after carburisation phenomena. A complementary microstructure characterisation is also presented. The atomic orbital occupations of the metallic bonds close to the C atom are affected. The main changes are presented in Ni 4s, Fe 4p and Cr 4p orbitals. An electron transfer to the C atom from the Ni, Fe and Cr nearest neighbour atoms is observed. The most affected is the strength of Fe—Ni, Cr—Ni, Ni—Ni and Fe—Cr bonds nearest neighbours to C atom. The metallic bond weakening is mainly a consequence of the new C–Ni, C–Fe and C–Cr interactions. The experiments in real-used samples show the formation of carbides and the loss in mechanical properties that can be explained on the bases metal-C bonds formation at expenses of metal–metal bonds.

Acknowledgements

This work was supported by SECyT UNS and UTN, PIP-CONICET 0103 and PICT 1770. The authors thank G. Brizuela and S. Simonetti, members of CONICET. The authors also thank the reviewers for their useful comments.

References

[1] U. Krupp and H.J. Christ, J. Phase Equilib. Diffus. 26 (2005), p. 5.
[2] N.K. Das, K. Suzuki, K. Ogawa, and T. Shoji, Corros. Sci. 5 (2009), p. 908.
[3] J.D. Tucker, T.R. Allen, and D. Morgan, Ab initio *defect properties for modeling radiation-induced segregation in Fe–Ni–Cr alloys*, Proceedings of the 13th International Symposium on Environmental Degradation of Materials in Nuclear Power Systems, Whistler, BC Canada, 19–23 August 2007.
[4] J.D. Tucker, R. Najafabadi, T.R. Allen, and D. Morgan, J. Nucl. Mater. 405 (2009), p. 216.
[5] L. Toft and L. Marsden, Iron Steel Inst. 70 (1961), p. 276.
[6] R. Yin, Materials at High Temperature 21 (2004), p. 111.
[7] Y. Nishiyama, Y. Sawaragi, and N. Otsuka, *Carburization resistance of Fe-25mass%Cr-38%Ni-1.8Si-1.5%Mo alloy in laboratory CH_4–CO_2–H_2 gas environments at 1000–1150°C*, Corrosion 2001, 11–16 March 2001, NACE International (2001).
[8] A.A. Kaya, P. Krauklis, and D.J. Young, Mater. Charact. 49 (2002), p. 11.
[9] A. Chauhan, M. Anwar, K. Montero, H. White, and W. Si, J. Phase Equilib. Diffus. 27 (2006), p. 6.
[10] R. Hoffmann and W.N. Lipscom, J. Chem. Phys. 36 (1962), p. 2179.
[11] R. Hoffmann, J. Chem. Phys. 39 (1963), p. 1397.
[12] M.H. Whangbo, J. Am. Chem. Soc. 100 (1978), p. 6093.
[13] A.B. Anderson, J. Chem. Phys. 62 (1975), p. 1187.
[14] G. Landrum and W. Glassey, *Yet Another Extended Huckel Molecular Orbital Package (YAeHMOP)*, Cornell University, Ithaca, NY, 2004.
[15] S. Armengol Gonzalez, *Caracterización microestructural y mecánica de barreras térmicas por APS y EB-PVD degradadas por fatiga térmica y por contacto, proyecto de fin de carrera Ingeniería de Materiales*, Universidad Politécnica de Cataluña, España, 2006.